Complex Lithiation Mechanism of Siloxene and Germanane: Two Promising Battery Electrode Materials

L. Loaiza, N. Dupre, C. Davoisne, Lénaïc Madec, L. Monconduit, V. Seznec

▶ **To cite this version:**

L. Loaiza, N. Dupre, C. Davoisne, Lénaïc Madec, L. Monconduit, et al.. Complex Lithiation Mechanism of Siloxene and Germanane: Two Promising Battery Electrode Materials. Journal of The Electrochemical Society, 2021, 168 (1), pp.010510. 10.1149/1945-7111/abd44a . hal-03134508

HAL Id: hal-03134508

https://hal.umontpellier.fr/hal-03134508

Submitted on 8 Feb 2021

HAL is a multi-disciplinary open access archive for the deposit and dissemination of scientific research documents, whether they are published or not. The documents may come from teaching and research institutions in France or abroad, or from public or private research centers.

L'archive ouverte pluridisciplinaire **HAL**, est destinée au dépôt et à la diffusion de documents scientifiques de niveau recherche, publiés ou non, émanant des établissements d'enseignement et de recherche français ou étrangers, des laboratoires publics ou privés.

Distributed under a Creative Commons Attribution 4.0 International License

Journal of the Electrochemical Society

The Electrochemical Society
Advancing solid state & electrochemical science & technology

OPEN ACCESS

Complex Lithiation Mechanism of Siloxene and Germanane: Two Promising Battery Electrode Materials

To cite this article: L. C. Loaiza *et al* 2021 *J. Electrochem. Soc.* **168** 010510

View the article online for updates and enhancements.

Discover the EL-CELL potentiostats

- Fully independent test channels with Pstat / GStat / EIS
- Optionally with integrated temperature controlled cell chamber
- Unique Connection Matrix: Switch between full-cell and half-cell control at runtime

www.el-cell.com +49 (0) 40 79012 734 sales@el-cell.com

EL-CELL®
electrochemical test equipment

This content was downloaded from IP address 88.127.95.218 on 08/02/2021 at 13:03

Journal of The Electrochemical Society, 2021 **168** 010510

Complex Lithiation Mechanism of Siloxene and Germanane: Two Promising Battery Electrode Materials

L. C. Loaiza,[1,z] N. Dupré,[2] C. Davoisne,[1,3] L. Madec,[3,4] L. Monconduit,[3,5] and V. Seznec[1,3]

[1]*Université de Picardie Jules Verne, Laboratoire de Réactivité et Chimie des Solides (LRCS), 80000 Amiens, France*
[2]*Institut des Matériaux Jean Rouxel (IMN), CNRS UMR 6502, Université de Nantes, 44322 Cedex 3 Nantes, France*
[3]*Réseau sur le Stockage Electrochimique de l'Energie (RS2E), FR CNRS 3459, Hub de l'Energie, 80000 Amiens, France*
[4]*CNRS/Université de Pau & Pays Adour/E2S UPPA, Institut des Sciences Analytiques et de Physicochimie pour l'Environnement et les Matériaux, UMR5254, 64000, Pau, France*
[5]*ICGM, Université de Montpellier, CNRS, ENSCM, 34095 Montpellier, France*

The layered siloxene and germanane, derived from $CaSi_2$ and $CaGe_2$, respectively, have shown very promising results as anodes for Lithium-ion batteries. Their delivered capacities, capacity retention and high rate cycling are superior compared to bulk Si and Ge. These positive features are most probably related to the layered morphology that buffers the volume changes and improves the kinetics. Despite numerous recently published studies regarding their electrochemical properties, very little is known about their electrochemical mechanism. In this work, we have used a combination of different characterization techniques to study the processes taking place during the lithiation of siloxene and germanane and compared with Si and Ge. Our results suggest a slightly different pathway for the lithiation of siloxene and germanane: their initial layered morphology is preserved after cycling, the crystalline $Li_{15}Si_4$ and $Li_{15}Ge_4$ characteristic of an alloying mechanism are absent and possibly different lithiated intermediates are formed. We provide then, an initial assessment of the involved Li_xSi and Li_xGe phases and propose the hypothesis of a reversible Li intercalation in the siloxene and germanane layers.
© 2021 The Author(s). Published on behalf of The Electrochemical Society by IOP Publishing Limited. This is an open access article distributed under the terms of the Creative Commons Attribution 4.0 License (CC BY, http://creativecommons.org/licenses/by/4.0/), which permits unrestricted reuse of the work in any medium, provided the original work is properly cited. [DOI: 10.1149/1945-7111/abd44a]

Manuscript submitted October 13, 2020; revised manuscript received December 3, 2020. Published January 7, 2021. *This paper is part of the JES Focus Issue on Selected Papers of Invited Speakers to IMLB 2020.*

Supplementary material for this article is available online

Silicon and germanium have emerged as potential candidates for LIB due to their high theoretical capacities, 3579 mAh g^{-1} ($Li_{15}Si_4$) and 1384 mAh g^{-1} ($Li_{15}Ge_4$).[1] Nevertheless, the high Li uptake brings up challenges such as volumetric expansion and/or unstable SEI layer, which are detrimental to the electrodes and leads to capacity fade. Different strategies have been proposed in the literature to overcome these issues, from the structural modification to the electrode and electrolyte formulation.[1] Likewise, it has been demonstrated that the use of a layered material can buffer the volume changes while improving the overall kinetics of the system.[2] Silicon and germanium present various compounds with layered structure, among them the siloxene and germanane, obtained after the topotactic deintercalation of Ca^{2+} from $CaSi_2$ and $CaGe_2$, respectively.[3,4] These compounds share a basic Si or Ge backbone composed of Si_6 or Ge_6 rings interconnected to form planes with Ca^{2+} intercalated for $CaSi_2$ and $CaGe_2$, –OH/–H for siloxene and only –H for germanane. These two last ones have found great applications in the field of optoelectronics due to their luminescence properties and only recently have attracted attention in the battery domain. We have previously reported their electrochemical performance as anode for Lithium-ion batteries (LIB), with improved results compared to bulk Si and Ge, in terms of delivered capacities, capacity retention and high rate cycling.[3,4] Other studies have also considered siloxene and germanane or their derivates as electrode materials with very promising results[5–10] but very little attention has been given to their electrochemical mechanism. Hence, the reasons behind their improved performance or the role of the layered morphology in the electrochemistry remain unknown. Indeed, it has been demonstrated that the structure, particle morphology and cycling conditions have a key role in the lithiated species formed during the cycling of Si and Ge and we believe that this might be the case for siloxene and germanane as well.[1,11] In this work we combine a series of characterization techniques such as, X-ray diffraction (XRD), Scanning and transmission electron microscopy (SEM and TEM), Raman and IR spectroscopy, X-ray photoelectron spectroscopy (XPS) and ^{6}Li Magic Angle Spinning Nuclear Magnetic Resonance (MAS NMR) to gather information about the lithiation of siloxene and germanane and compare the results with previous reports for Si and Ge. Our findings suggest a different behavior for the lithiation of siloxene and germanane compared to bulk Si and bulk Ge. Particularly, the characteristic features for the alloying reaction are almost absent and evidence points to the preservation of the initial layered morphology. This information led us to propose the hypothesis of a possible intercalation of Li in the siloxene/germanane layers, although further experiments are needed to confirm it. This work, then, sets the basics for the understanding of the processes taking place in layered siloxene and germanane in order to unfold their true potential as energy storage materials.

Experimental

Electrode preparation.—The electrodes were prepared with a weight ratio was 1:1:1 of active material (siloxene/germanane), C_{45} conductive additive and CMC (carboxymethyl cellulose) binder (CMC-DS = 0.9, Mw = 700 000 Aldrich). The active material was pre-mixed with the carbon additive by SPEX for 10 min using 1 ball per 100 mg of total mass. Following, the resulting powder was mixed with the binder using a mortar and 1 ml of distilled water with 0.1% of Triton X dispersant. The slurry was magnetically stirred for one night and casted either onto a Cu or a Mylar foil (self-supported electrode—to rule out the contribution of the Cu current collector to the different characterizations), using a Doctor Blade (100 μm thickness), dried under ambient conditions for one day and vacuum dried at 70 °C overnight.

In situ XRD.—The diffractograms were recorded in a Bruker D8 Advanced diffractometer with Cu radiation ($\lambda 1$ = 1.54056 Å, $\lambda 2$ = 1.54439 Å), using a specifically designed cell with Be window.[12] The cell was assembled with a self-supported electrode, using 1 M $LiPF_6$ in EC/DMC with 1% FEC, a Whatman glass fiber separator

[z]E-mail: laura.loaiza@chalmers.se

and Li metal as a counter electrode. To ensure a complete stabilization of the intermediates, the cycling was performed at C/40 (C/n = 1Li /n h) vs Li/Li^+. The diffraction patterns were recorded at a set potential, in a 2θ range of 8°–40° for one hour.

Ex situ characterizations.—Self-supported electrodes were cycled in Swagelok cells, with 1 M $LiPF_6$ EC/DMC + 1%FEC, a Whatman glass fiber separator and Li metal as a counter electrode, at a rate of C/20 (C/n = 1Li /n h) between 0.001–2.0 V vs Li/Li^+. The electrodes were recovered inside an Ar-filled glove box, washed with DMC and dried under vacuum.

The cycled electrodes were characterized by *Raman spectroscopy* using a DXR 2 Raman Microscope spectrometer (Thermo-Fisher Scientific, 532-nm excitation). In order to avoid contact with air, the samples were placed in a glass lid and sealed with Kapton foil. The Fourier Transformed *Infrared spectroscopy* was performed using KBr methods and a cell with NaCl window to avoid sample contact with air. The morphology and composition were analyzed by *Scanning Electron Microscopy SEM* (SEM-environmental FEI Quanta 200 FEG) and *Energy Dispersive X-ray EDX* (X INCA Oxford). The *Transmission Electron Microscopy (TEM), Scanning Transmission Electron Microscopy (STEM)* and *Electron Energy Loss Spectra (EELS)* were performed in a TEM-FEI Tecnai F20 S-TWIN, operating at 200 kV fitted with a Gatan Image Filter Tridiem in post column. The electron diffraction patterns were obtained with Selected Area Electron Diffraction (SAED). The EELS was performed with 1–2 eV energy resolution, a dispersion of 0.2 eV ch^{-1}, a conversion and a collection angle of 5.8 and 2.2 mrad, respectively. The energy loss near edge structure (ELNES) acquisitions were performed in STEM mode in defocus to limit the electron beam interaction. All the energy losses presented an error of ±0.2 eV. The EDX was acquired in order to determine the local chemical composition. The air sensitive samples were prepared in an Ar filled glove box and transferred to the TEM under an Ar flow.[13] The *X-ray Photoelectron Spectroscopy (XPS)* was performed using a Escalab 250 Xi spectrometer with a monochromatized Al Kα radiation ($h\nu$ = 1486.6 eV). The electrodes were placed on a sample holder using an insulating uPVC tape (ref. 655 3 M) and then transferred to an Ar-filled glove box directly connected to the spectrometer. The analyses were performed with the standard charge compensation mode and an elliptic 325 × 650 μm X-ray beam spot. Core spectra were recorded using a 20 eV constant pass energy with a 0.10 eV step size and short time iterative scans. The *^{6}Li and ^{1}H Nuclear Magnetic Resonance (NMR)* were performed with a Bruker Avance-500 spectrometer (B_0 = 11.8 T) using a Bruker MAS probe with a 2.5 mm diameter zirconia rotor. Spinning frequencies up to 25 kHz were used. ^{6}Li NMR (Larmor frequency $\nu_0(^6Li)$ = 73.59 MHz) spectra were acquired with a single pulse sequence and a recycle time of 30 s. All spectra displayed in this work were normalized considering the number of scans, the received gain and the mass of the sample. ^{6}Li integrated intensities were determined by using spectral simulation (Dmfit software[a]) and are given in a.u. for comparison purpose.

Results and Discussion

Previously, we have reported the synthesis and electrochemical properties of siloxene and germanene.[3,4] Their galvanostatic cycling suggested a different profile compared to bulk Si and bulk Ge. Indeed, their electrochemical mechanism is related to their structure and cycling conditions, meaning that different crystalline or amorphous lithiated phases can be stabilized.[11] By a combination of different characterization techniques we have identified the similarities and differences between the electrochemical lithiation mechanisms of siloxene and germanane with previous reports on bulk Si and Ge.

Firstly, an in situ XRD experiment was performed on siloxene and germanane film cycled vs Li^+/Li^0, to identify the possible presence of any $Li_{15}X_4$ -type (X = Si, Ge) crystalline phase,

[a]D. Massiot. http://nmr.cemhti.cnrs-orleans.fr/dmfit/.

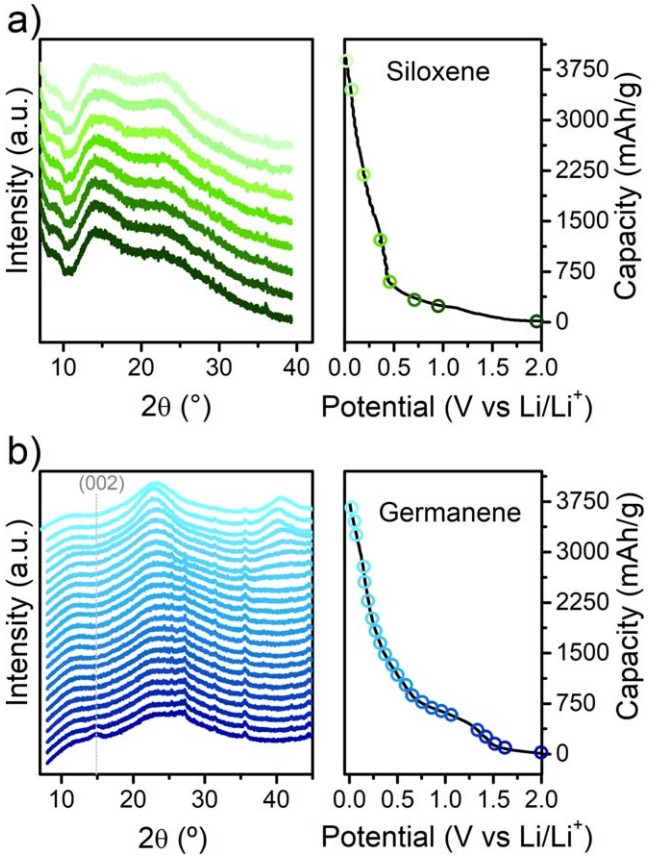

Figure 1. In situ XRD for a self-supported (a) siloxene and (b) germanane electrode cycled vs Li at C/40.

characteristic of the alloying reaction with Li (Fig. 1). The experiments were performed at a low C rate of C/40, in order to allow the stabilization of the different phases. Figure 1a shows the lithiation of siloxene, most of the XRD patterns are mainly amorphous and only a very huge hump is observed centered at 15°. At potentials lower than 100 mV, no crystalline phase is observed, contrary to the findings for bulk Si where the crystallization of $Li_{15}Si_4$ takes place,[14] instead, a second hump appears at around 22.5°. These observations are consistent with Gao et al.[15] who after lithiation identified broad and less intense siloxene XRD peaks, accompanied by two broad humps at 15° and 22.5°. Figure 1b presents the in situ XRD of germanane, here the increased number of electrons in Ge allowed a stronger diffraction and it was possible to observe the (002) Bragg reflection. This peak is visible until ≈1.5 V, following there is an amorphous region until ≈0.4 V, where humps appear at around 23° and 40°. These humps increase in intensity as the potential decreases and by the end of discharge they have transformed into very broad peaks that shift towards lower angles and later to higher angles before the end of discharge. These broad peaks are not related to the presence of $Li_{15}Ge_4$ or $Li_{17}Ge_4$ and might correspond to weakly crystallized Li_xGe phases with different lithiation degrees. As we have previously reported,[11] Ge is particularly sensitive to the cycling conditions and different stoichiometries can be stabilized during the lithiation. We believe that germanane is not the exception and more than one weakly crystallized lithiated phase can be present at a given stage.

Raman spectroscopy was used as a complementary technique to study the system. Figure 2a show the Raman spectra for the $CaSi_2$, siloxene and lithiated/delithiated siloxene. All of them present the same basic structure of Si–Si bonds in Si-planes defined by an intense peak centered between 492–507 cm^{-1} and the second order TA and TO at 283 and 900 cm^{-1}. Upon Ca deintercalation from $CaSi_2$ to form siloxene, new bands appear at 635, 735 and

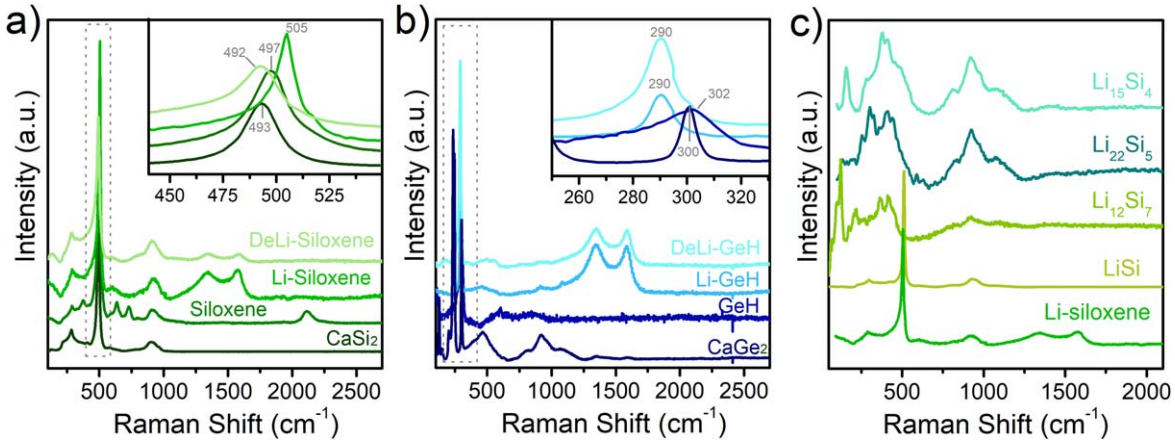

Figure 2. Raman spectra of (a) $CaSi_2$, siloxene and lithiated/delithiated siloxene and (b) $CaGe_2$, germanane and lithiated/delithiated germanane and (c) lithiated siloxene compared with LiSi, $Li_{12}Si_7$, $Li_{22}Si_5$, $Li_{15}Si_4$.

2115 cm^{-1}, ascribed to the Si–H vibrations. These bands disappear upon electrochemical (de)lithiation. The Infrared spectroscopy results (Fig. S1 is available online at stacks.iop.org/JES/168/010510/mmedia) corroborate these findings and show a decrease in intensity of the –OH bands, particularly for the delithiated siloxene. Interestingly, the Si planes Raman vibration modes and the Si–O–Si, H–Si–O IR bands are preserved, possibly indicating no structural degradation or/and formation of Li-silicates upon cycling. Additional Raman bands emerge at 1330/1600 cm^{-1} corresponding to the disordered (D) A_{1g} breathing mode of defects/vibrations and the graphitized (G) E_{2g} vibration of the C–C plane from the conductive carbon[16] and IR bands at 1445/1310 cm^{-1}, ascribed to the electrolyte decomposition products (1650 (C=O), 1398 (C–H), 1300 (C=O) cm^{-1}).[16]

The main Si–Si planes Raman band position appears to be related with the cation type; for $CaSi_2$ it is centered at 493 cm^{-1} and at 497 cm^{-1} once the Ca is replaced by –H and –OH in siloxene. Upon lithiation it shifts to 505 cm^{-1} and after delithiation to 492 cm^{-1}. This shift could be related with a change in the interlayer separation, for $CaSi_2$ only one Ca^{2+} is intercalated, for siloxene there are –H/–OH above and below the planes, which are probably substituted by Li in the lithiated siloxene. These changes increase the interlayer distance and result in a Raman shift. Note that several experiments were performed in order to rule out possible interferences due to sample inhomogeneity, in all cases the trend was similar. This phenomenon was further investigated by in situ Raman spectroscopy (Fig. S2). Despite the poor signal/noise result caused by the cell configuration it can be observed that the Si–Si band is maintained all along the discharge, yet with low intensity at the end of discharge.

Following, the Raman spectra of the lithiated siloxene was compared with different lithiated references prone to be formed during the lithiation ($Li_{15}Si_4$, $Li_{22}Si_5$, $Li_{12}Si_7$) (Fig. 2c). Only the LiSi spectrum resembles the one of lithiated siloxene, although the main bands are centered at different wavelengths (511 cm^{-1}-LiSi and 505 cm^{-1}-Li-siloxene).[17] The LiSi has several layered polymorphs, one of them with the same Si_6 rings planes as in siloxene.[18] Its theoretical capacity is 954 mAh g^{-1}[19] which is lower than the capacity values obtained for siloxene (2300 mAh g^{-1}),[4] meaning that possibly both structures resemble but somehow the siloxene is able to store more lithium, or other Li_xSi phases are involved.

The Raman spectrum for the pristine germanane (Fig. 2b) shows only one peak centered at 302 cm^{-1}, assigned to the Ge-Ge bonds in the planes. Upon lithiation/delithiation, this peak shifts to 290 cm^{-1}, and the D and G bands from the carbon additive appear at 1330 and 1600 cm^{-1}. Contrary to the siloxene this Raman shift is not reversible after Li deinsertion. The redshift of the Ge–Ge peak suggests a change in the interlayer distance that could be also related with the presence of mainly Ge–H bonds and few/no Ge–OH, as germanane has a preferential bonding with –H (Fig. S1b).[20] similar findings have been reported in the literature, where a broad band at 269 cm^{-1} was attributed to the amorphization of germanane, caused by the oxidation and dehydrogenation after cycling.[7]

To further investigate the preservation of the siloxene and germanane planes, SEM and TEM imaging was performed on the electrodes after Li-ion extraction and insertion (Figs. 3, S3, S4). The particles have an inhomogeneous size distribution with several

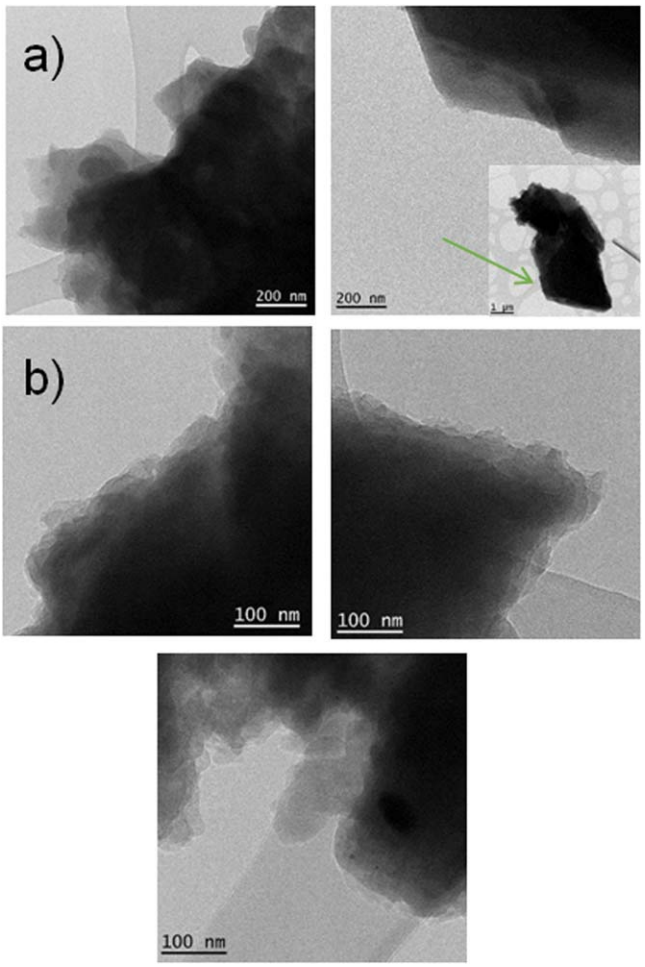

Figure 3. TEM images of the lithiated electrode of (a) siloxene and (b) germanane.

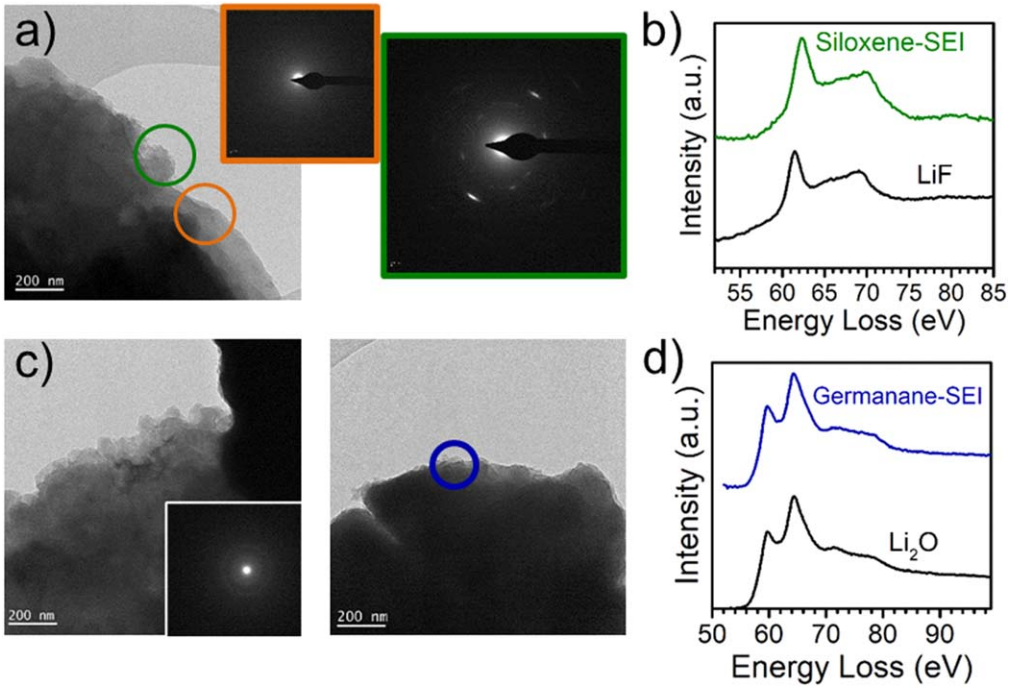

Figure 4. TEM picture of (a) a lithiated siloxene electrode and the electron diffraction obtained for two different surface morphologies, one showing an amorphous character, the other one a crystalline pattern, (b) EELS spectra for the area for which a crystalline electron diffraction was obtained, confirming the presence of LiF. TEM images of a lithiated germanane electrode displaying its corresponding (c) electron diffraction pattern with an amorphous character and (d) the EELs spectra of the area highlighted in orange showing the presence of mainly Li_2O.

lateral sizes formed of various stacked layers surrounded by the carbon conductive additive and covered by a decomposition layer. In all cases, remains of the layered morphology are observed, in agreement with the reports from Pazhamalai et al.[21] For germanane some of the layers are exfoliated and the edges are smoothed, probably due to the formation of a passivation layer on the surface, which appear to be thicker compared to siloxene. A deeper analysis of the particles surface revealed some differences; in siloxene two different morphologies consisting of multiple nanocrystals and a smooth layer are found (Fig. 4a). The first one is ascribed to the presence of polycrystalline LiF based on the electron diffraction and EELs results (Fig. 4b), while the second one has an amorphous character. The germanane decomposition layer is also composed of multiple particles, which are amorphous (Fig. 4c) and correspond mainly to the presence of Li_2O as observed by EELs (Figs. 4c, 4d). Possibly, the preferential bonding of germanane with –H over –OH

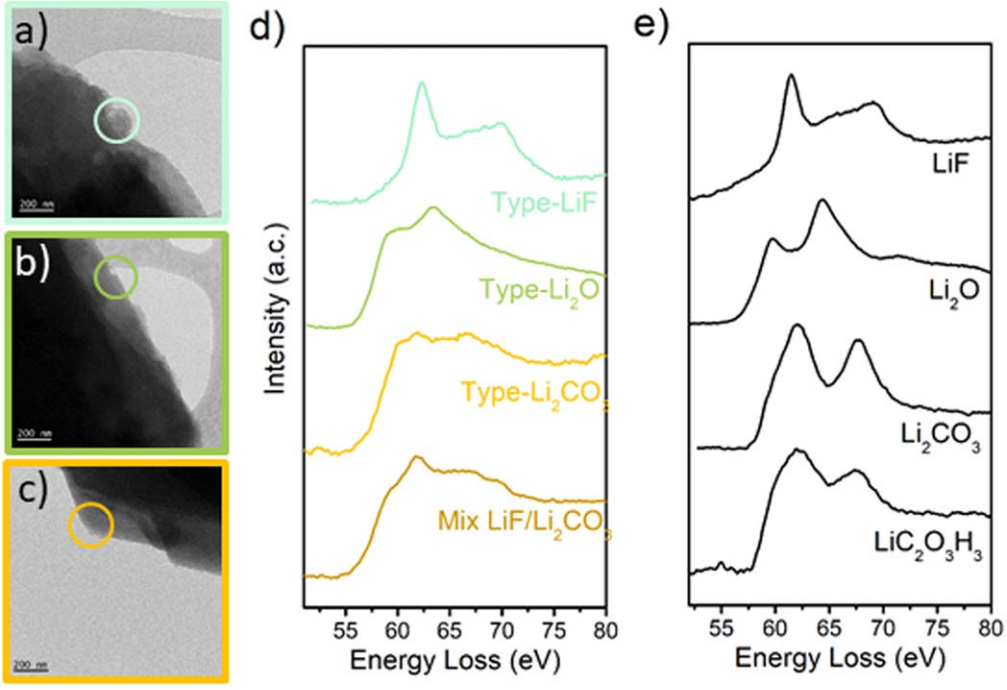

Figure 5. TEM images of the lithiated siloxene with regions of different composition of the SEI layer, (a) type-LiF, (b) type-Li_2O and (c) type-Li_2CO_3, (d) their corresponding EELS spectra and (e) EELS spectra of the reference compounds.

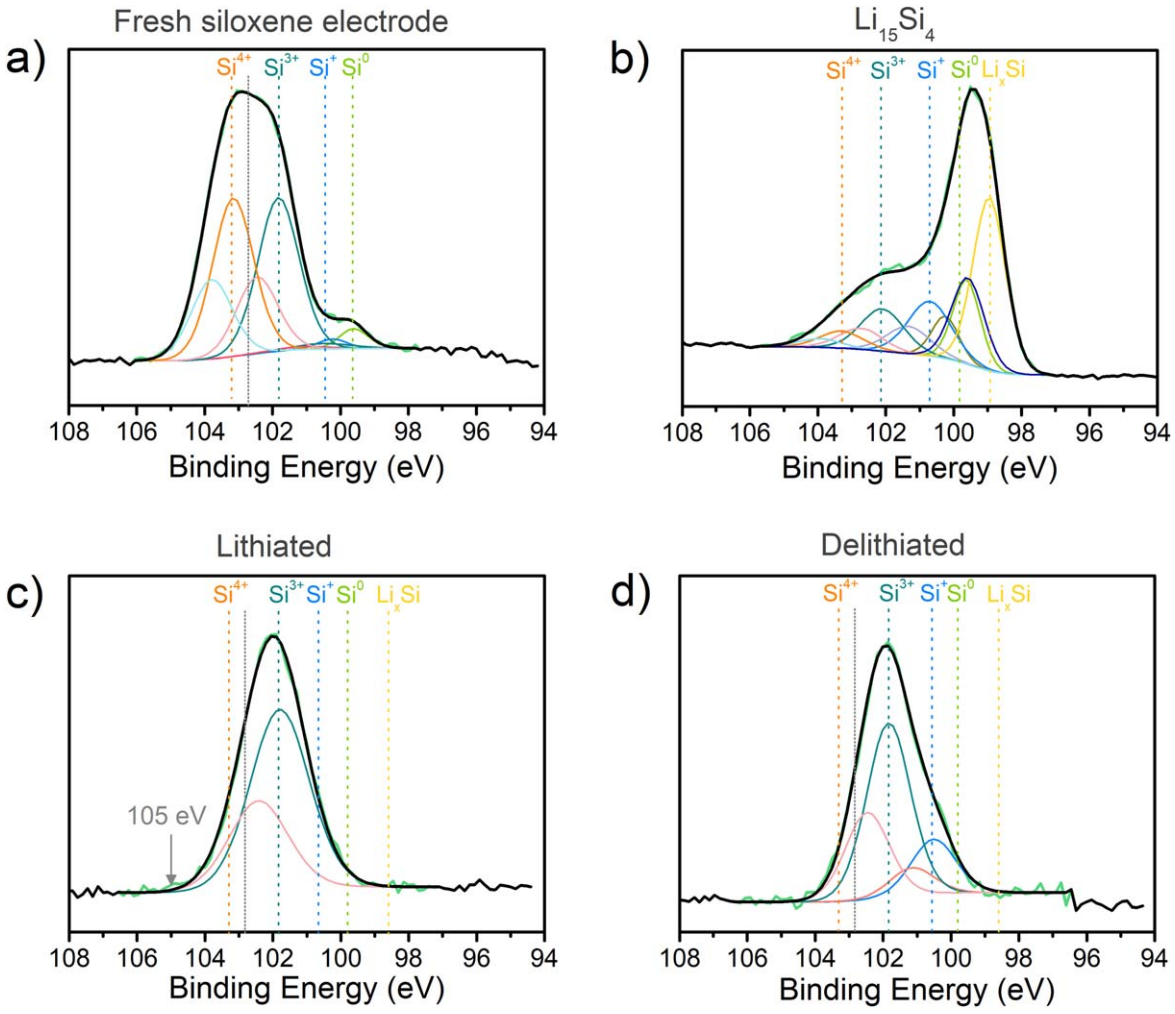

Figure 6. XPS spectra of (a) pristine siloxene electrode, (b) mechanically synthesized $Li_{15}Si_4$ reference, (c) lithiated siloxene and (d) delithiated siloxene.

has an impact on the different decomposition products formed upon cycling. Interestingly, in siloxene, the amorphous compound is found in the areas in which the sharpness of the layers is preserved.[22] An EELs study in these areas (Fig. 5) revealed the presence of various signals corresponding to Li_2O (Li K- edge double band at 60.1 and 64.5 eV), lithium-carbonate type Li_2CO_3 or methyl lithium carbonate ($LiC_2O_3H_3$)[23] (double band at 62.3 and 67.5 eV) and a mixture of multiple contributions type lithium oxide, lithium carbonate and lithium fluoride. An additional contribution present in all the spectra is possibly related to the Li in the siloxene layer. Unfortunately, due to the penetration depth the EELS and the significant thickness of the SEI layer, an analysis of the bulk of the layers was not possible. The composition of the SEI layer appears then to be inhomogeneous with local variations and areas with non-lithiated compounds, as previously observed for other Si-based electrodes.[24]

The EELS spectra at the Si-edge (Fig. S5) has been also analyzed for pristine siloxene. It presents the characteristic signal from Si^{4+}.[5,15] For the discharged siloxene electrode, the shoulder at low energy that accompanied the peak at 110 eV disappears and is replaced by a shoulder at high energy. This change in profile could be an indicator of the presence of Li in the siloxene layers or could also come from a decomposition product type-Li_ySiO_x. The analysis also showed the presence of areas without lithium, depicting an inhomogeneous lithiation process.

In order to further investigate this decomposition layer and gather information about the presence of Li inside the siloxene layers, X-ray Photoelectron Spectroscopy (XPS) was performed. In general, the Si2p states of siloxene can be resolved into two main components: Si–Si and Si–O_x bonding. A comparison with the as-prepared electrode reveals changes in the profile after the electrode preparation (Fig. S6); Si–O_x bonds increased due to the aqueous electrode formulation with CMC binder while the Si^0 and Si^+ peak intensity decreases revealing a loss in the fraction of the Si-H bonds.[9,21,25] The former most probably comes from the formation of Si_2O_3 suboxides and their disproportionation reaction[26] while the latter is an indicator of an oxidation process.[6] Note that the Si–O binding energies are slightly different compared to bulk SiO_2 (104 eV), suggesting the presence of different compounds, [27] which are likely highly influenced by the siloxene surface activity.[28] All these variations induced by the electrode preparation have been reported for other Si-based electrodes using CMC and water as a solvent and can be attributed to bonding between the CMC and the siloxene surface.[29] Table SI summarizes the peak position and atomic concentration for the as-prepared electrode.

Following, the lithiated and delithiated siloxene electrodes were analyzed (Fig. 6). Note that the significantly thick decomposition layer (as observed in TEM) hinders the access of the X-ray beam. After the lithiation (Fig. 6c), the Si^0 and Si^+ peaks are no more visible and only the Si^{3+} peak is preserved, in line with previous reports on Si based electrodes.[10,24,29,30] The Si^{3+} peak can be attributed to the transformation of SiO_x into $Li_xSi_yO_2$, or to lithiated electrolyte decomposition products.[24,30] The Si^+ observed after delithiation could be originated from $Li_xSi_yO_2$ or Si–OH. The ratio between these peaks and their position depend on the morphology, surface reactivity, interactions between Si and the decomposition

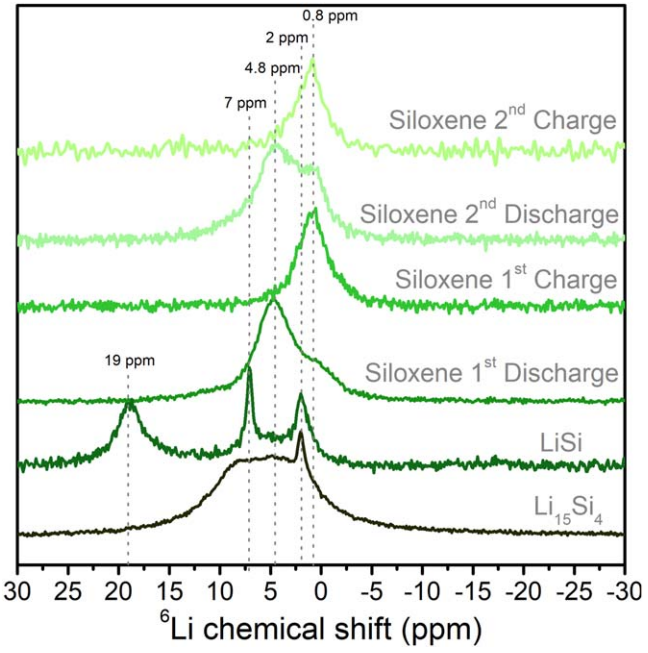

Figure 7. ^{6}Li NMR spectra of the 1st and 2nd lithiation/delithiation of a siloxene self-supported electrode and the LiSi and $Li_{15}Si_4$ references synthesized by ball milling.

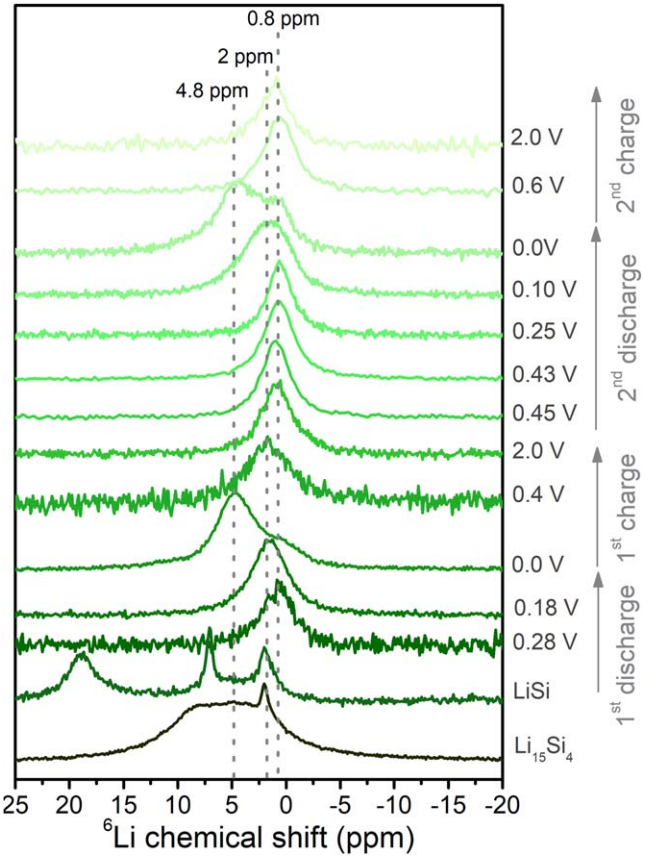

Figure 8. ^{6}Li NMR spectra of a self-supported siloxene electrode cycled at different depth of discharge/charge and the LiSi and $Li_{15}Si_4$ references synthesized by ball milling.

products and degree of lithiation/delithiation. Further analysis must thus be performed, e.g. sputtering the surface to remove the SEI layer but this could induce some degradation of the lithiated phases. For comparison, a mechanically synthesized $Li_{15}Si_4$ reference was analyzed (Fig. 6b, Table SII and showed the presence of Si^0, Si^+, Si^{3+} and Si^{4+}, and an additional peak at 98.95 eV, ascribed to a Li_xSi phase. For the delithiation (Fig. 6d), the Si^{3+} and Si^+ peaks are observed. Note that experiments performed with an Ag Lα source at 2984.2 eV, enabling probe about two times depth, performed on the lithiated siloxene, did not reveal any Li_xSi peak, indicating that the SEI is very thick.

Finally, MAS NMR was performed in order to access the bulk of the lithiated/delithiated siloxene and germanane. ^{6}Li NMR was preferred over ^{7}Li due to its higher resolution, despite its lower abundance and longer relaxation times. Its smaller quadrupole and gyromagnetic moments compared to ^{7}Li typically result in spectra that are easier to interpret.[31,32] Figure 7 shows the MAS ^{6}Li NMR spectra for the lithiated/delithiated siloxene anode for the first and second cycle, compared to the mechanically synthesized LiSi and $Li_{15}Si_4$ references. Two main Li environments can be identified; the first one at approximately 0.8 ppm is attributed to the SEI layer and the second one at 4.8 ppm to a Li_xSi phase formed during the reduction. The lithiated siloxene presents both resonances, while for the delithiated sample only the one close to 0.8 ppm is observed, meaning that most of the signal is coming from the SEI or from Li stored or trapped in the surface of the layers. Note that for the second lithiation the intensity of the 0.8 ppm resonance increases by a factor of 1.5. This variation could be originated from a difference in the electrochemistry of the cells (despite their general reproducibility), rather than an additional formation of SEI layer. Indeed, for all the cells, most of the capacity is obtained below 0.2 V, except for the cell disassembled at the first discharge, which reached a higher reversible capacity at high potentials with lower formation of SEI layer. This is consistent with the peak deconvolution and quantification of the different components presented in Table SIII, where the SEI signal changes for the first discharge/charge cycle from 3.76 to 5.71 a.u, whereas for the second one from 6.6 to 6.59 a.u.

The LiSi reference presents three relatively sharp bands at 19, 7 and 2 ppm while the $Li_{15}Si_4$ is composed of a sharp peak at 2 ppm and a very broad signal centered between 5–10 ppm. For LiSi the resonance at 19 ppm (40%) is assigned to the presence of Li in Si clusters, like $Li_{12}Si_7$ (composed of Si_5 rings and Si_4 stars) or other poorly lithiated phases and the one at 7 ppm is likely originated by a more lithiated environment. Two additional broad signals are found at 4.5 ppm (Si^{4-} isolated ions ($Li_{15}Si_4$)) and 11.8 ppm (LiSi[29] or $Li_{13}Si_4$).[32,33] The LiSi phase has a peculiar structure for a monosilicide: while NaSi and KSi have only isolated Si^{4-} ions, the LiSi presents different polymorphs, among them, one composed Si sheets of interconnected Si_6 rings like in silicene or siloxene.[18] The different polymorphs can be stabilized depending on the synthesis conditions and various Li environments are expected. Probably, the different resonances observed in the NMR spectra at 11.8 and 7 ppm, could be also related with the presence of a certain polymorphs. For $Li_{15}Si_4$, the peak at 5–10 ppm can be deconvoluted into two contributions, one at 5–6 ppm (78%) corresponding mainly to isolated Si^{4-} ions ($Li_{15}Si_4$)[32–36] and the other one at 9 ppm (16%) to both isolated Si^{4-} ions and small Si clusters (dumbbells), like in $Li_{13}Si_4$. Indeed, $Li_{13}Si_4$ has been previously identified as a decomposition product of the metastable $Li_{15}Si_4$.[33] Both compounds present a resonance at 2 ppm, ascribed to a non-identified lithiated phase. This resonance has been also observed in the case of lithiated nanosilicon electrodes and assigned to a Li-rich phase.[24] A comparison of the Li_xSi from siloxene with the references suggests that both $Li_{15}Si_4$ and LiSi resonances can be comprised in the lithiated siloxene, but other phases with similar Li environments may coexist at this stage.

Subsequently, various cells were stopped at different depth of discharge/charge (Fig. 8). At the beginning of the lithiation (0.28 V), only one peak is observed at 0.8 ppm, ascribed to the formation of the SEI species. Further down in potential, at 0.18 V, the main peak is centered at 1.7 ppm, and at the end of the discharge the main resonance can be deconvoluted into two contributions: a major one

at 4.8 ppm with a very broad resonance at 11 ppm partially masked. These signals are accompanied by the shoulder at 0.8 ppm, assigned to SEI species. For the delithiation, at 0.4 V the 4.8 ppm peak disappears and leaves place to a broad signal comprised of signals at 2.2 ppm and most likely 0.8 ppm. At 2.0 V, a slight apparent shift can be observed towards the 0.8 ppm position indicating that the 2.2 ppm signal eventually fades and at the end of charge only the signal of the SEI is observed. During the second discharge, at 0.45 V, the spectrum is composed of a main resonance at ≈0.8 ppm with a minor contribution (12%) at approx. 2 ppm, while at 0.43 and 0.25 V only the former is observed. At 0.10 V there is a broad signal, composed of contributions at 11, 4.8, 2.2 and 0.8 ppm and at the end of the second discharge, there are two peaks at 4.8 and 0.8 ppm. For the second charge, at 0.6 V, only a peak at 0.8 ppm is present and prevails until the end of charge. The peaks at 1.7, 2.2, 4.8 and 11 ppm can be attributed to the presence of Li_xSi phases and are discussed below.

Note that the lithiation of bulk Si proceeds via breaking of the Si crystalline network into small clusters, reflected in the NMR spectra by a continuous shift of the resonances to lower frequencies as the cluster size is reduced and the Li/Si ratio increased. Typically, Li environments with big Si clusters (lithium poor Li-Si alloys) give signals between 16–22 ppm, small Si clusters or dimmers between 12–14 ppm, small clusters and isolated Si^{4-} ions between 8–10 ppm and only isolated Si^{4-} (lithium rich Li–Si alloys) between 3–6 ppm. An overlithiated non-stoichiometric phase $Li_{15\pm\delta}Si_4$ has been detected at approx. −10 ppm.[35,36] For the lithiated siloxene, no resonance above 15 ppm could be found, implying that no big cluster or low coordinated Li are involved. The process of overlithiation of $Li_{15}Si_4$ into $Li_{15\pm\delta}Si_4$ was also not observed.[34] Alternatively, three main signals are present at 11, 4.8 and 2.2 ppm. The resonance at 11 ppm is most likely related to LiSi, while the one at 4.8 ppm with Li_xSi phases probably with isolated Si^{4-} ions in their structure but other Li environments are possible. Note that the siloxene presents a small amount of c-Si, thus a certain content of $Li_{15}Si_4$ is expected. The 2.2 ppm peak could be related with some Li on the surface, diamagnetic species or Li_2O species in the SEI layer (signal usually rising at 2.8 ppm and identified by our EELs analysis).[19,35,37] Additionally, it could be linked with Li next to a big cluster or with high coordination number. Indeed, the theoretical studies suggest that the most thermodynamically stable coordination site for Li in silicene (Si monosheet) is the hollow center of the Si_6 ring, meaning that Li would have a coordination number of six. A similar resonance has been identified as a rich Li_xSi alloy for the lithiation of nanosilicon and Si nanowires with crystalline core and amorphous shell.[24]

This information suggests first that the lithiation of siloxene is highly reversible. Second that siloxene undergoes a slightly different mechanism compared to Si with the formation of at least three different Li_xSi species, some where the lamellar structure is preserved. The presence of the resonance at 4.8 ppm is commonly associated with isolated Si^{4-} ions, like in $Li_{15}Si_4$, but the broadness of the signal and the fact that this phase was not identified by other characterization techniques, indicate that other Li environments are possible. The formation of these phases does not seem to follow a specific pattern, and they can coexist at a certain voltage, e.g. 0.10 V (second discharge).

The germanane was also analyzed by ^{6}Li NMR (Fig. 9) during the first discharge/charge cycle at different voltages. During the first lithiation, at 0.40 V, the peak deconvolution suggests the presence of at least three resonances, close to 0 ppm, between 0.7 and −0.4 ppm. At 0.18 V, the peak is composed of signals at 6.7, 1.8 and the contribution close to 0 ppm already observed at 0.40 V. At the end of the lithiation two strongly overlapping signals are observed, one centered at 0 ppm and the other one appearing as a shoulder at 1.97 ppm, a last broad and intense signal at 7 ppm also emerges. Upon delithiation, the spectrum shows two main peaks at 1.8 ppm and −0.4 ppm. In order to assign the origins of these resonances it is worth to review the existing literature for the lithiation of

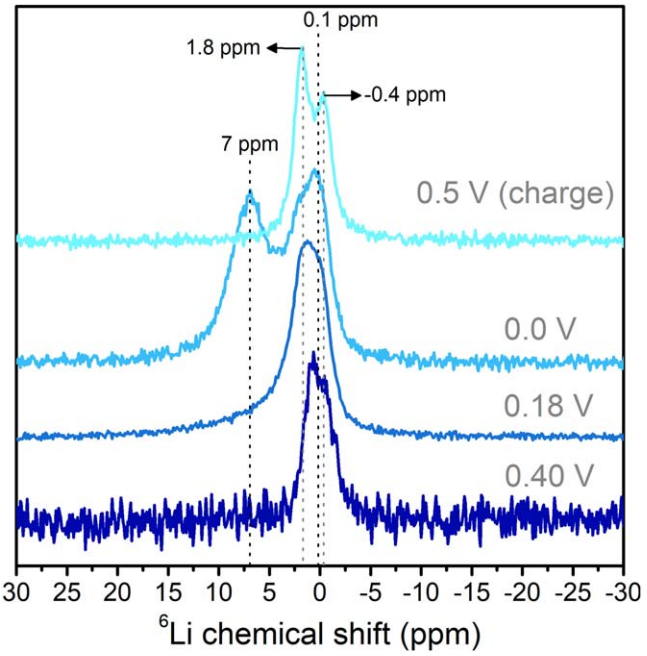

Figure 9. ^{6}Li NMR spectra for a self-supported germanane electrode cycled at different depth of discharge/charge.

germanium. This process happens in a similar way compared to silicon, with the breaking of the crystalline network as Li is incorporated until the formation of isolated Ge_4^{4-}. Signals between 20–25 ppm are related with Ge dumbbells (Li_7Ge_3 and Li_9Ge_4), 12–14 ppm to dumbbells and isolated Ge^{4-}ions (Li_7Ge_2 and $Li_{13}Ge_4$), 0–10 ppm to isolated Ge ions ($Li_{15}Ge_4$) and from –24 to −21 ppm to the process of overlithiation of $Li_{15}Ge_4$ into $Li_{15+\delta}Ge_4$.[38,39] Nonetheless, the Li_xGe intermediate phases are highly dependent on the cycling conditions, often they have similar formation energies and/or are metastable, thus multiple intermediates can be involved and be stabilized from their local structural resemblances rather than from the corresponding thermodynamic phases. For instance, $Li_{15}Ge_4$ is stabilized from the metastable $Li_{13}Ge_4$ and Li_7Ge_2 and not from the thermodynamic phases $Li_{13}Ge_5$ or Li_8Ge_3.[18,38–45] As a consequence, multiple alternatives proposed for the lithiation mechanisms can be found in the literature. In the case of germanane, all of the samples present a resonance close to 0 V which most probably correspond to lithiated species in the SEI layer and highly disordered phases or diamagnetic Li^+ components, which shift slightly as function of the state of charge.[38,39] For instance, ^{7}Li NMR signals for Li_2O, LiF and LiOH are typically rising at 2.8 ppm, −1.1 ppm and 0.4 ppm, respectively.[39,46] Also, Li^+ located near a π electron cloud is known to produce negative shifts.[47] The other peaks at 0.7–2 ppm and 6.7–7 ppm are related to the presence of Li_xGe species, the assignment of these resonances is complicated without further experiments, as they can be produced by several phases with similar formation energies and Li environments (Li_7Ge_3, Li_5Ge_2, $Li_{13}Ge_5$, Li_8Ge_3, $Li_{13}Ge_4$, $Li_{15}Ge_4$). Yet, the bands at 0.67–2 ppm are most probably related with Li in a shielded or high coordinated Li environment, like Li close to the germanane layers, in analogy to the analysis performed for siloxene. Likewise, Scherft et al.[47] have attributed the band at 2.1 ppm to $Li_{14}Ge_6$. Regarding the bands between 6.7–7 ppm, it could be produced by a phase with small Ge clusters and/or isolated Ge_4^{4-} or by a totally new phase. Since no evidence of crystalline $Li_{15}Ge_4$ (typical of an alloying mechanism) was found in our experiments, neither by XRD nor by ^{6}Li NMR (carbon-Ge nanotubes 10 ppm, micrometric Ge −13 ppm),[38,39] it is worth to consider also the hypothesis of a reversible Li intercalation in the germanane layers. Indeed, it has been theoretically studied for germanene (germanane monolayer).[48,49] The calculations indicate the

intercalation of 1 Li per Ge atom, forming LiGe. This phase has several polymorphs, one of them constituted of Ge^{-} ions built up in puckered six-membered rings of distorted chairs, stacked above each other in a staggered fashion.[50] Here, Li^{+} lies in the centre of a three-connected Ge^{-} hexagonal channels and is coordinated to other 8 Ge^{-} and each Ge^{-} is coordinated with 8 li^{+} (8:8).[51] Such type of structure could explain the resonances close to 2 ppm in germanane, corresponding to a highly shielded environment.

Conclusions

Siloxene and germanane are very promising candidates as anodes for different battery technologies, it is expected that their layered morphology buffers the volume variations during lithiation and allows fast Li ion diffusion, although before their commercialization several issues must be solved. In this study we have particularly inquired the processes taking place during lithiation/delithiation. Our findings suggest a different behavior compared to bulk Si or Ge. First, no evidence of crystalline $Li_{15}Si_4$/$Li_{15}Ge_4$, characteristic of the alloying with Li, has been found in siloxene nor germanane. The initial layered morphology is preserved as indicated by the different imaging techniques and Raman spectroscopy. A thick decomposition layer is deposited on the particle surface upon lithiation. This SEI layer presents local variations in the composition and different species are formed (Li_2O, LiF, Li-carbonates, Li-alkoxides, Li-esters) which are possibly related with the loss of the –H/–OH bonding upon lithiation. The process of lithiation appears to be inhomogeneous and some particles do not participate in the reaction. At least three different Li_xSi/Li_xGe phases are involved in the lithiation process, unfortunately, it was not possible to identify them. Evidence points out to the presence of a phase where the lamellar morphology is preserved, like LiSi and LiGe polymorphs with similar structure and environments to the basic Si/Ge backbone of siloxene and germanane. Theoretical calculations foresee that Li intercalation is achievable without kinetic limitations, structure degradation and volume expansion in a single layer of siloxene (silicene) and germanane (germanane)[37,52–55] and probably this could be true for bulk siloxene and germane. The expected full lithiated state is 1 li per 1Si/1Ge atom, resulting in a smaller theoretical capacity compared to the experimental capacity values obtained for siloxene and germanane, hence, apart from LiSi and LiGe other phases might be involved as well, as indicated by the NMR results where more than one resonance was identified. The presence of the NMR signal commonly associated with Si_4^{4-}/Ge_4^{4-} isolated ions, could refer to the formation of $Li_{15}Si_4$/$Li_{15}Ge_4$, but other unknown phases with similar Li-environment can produce similar signals. Based on this information, we have decided to consider the possibility of Li intercalation in the siloxene/germanane layers. Notwithstanding, an alloying mechanism could take partially place up to some extent if one considers the NMR signal associated with Si_4^{4-}/Ge_4^{4-} isolated ions ($Li_{15}Si_4$/$Li_{15}Ge_4$).

Undoubtedly, further analysis must be performed on the system, possibly combining calculations for a better interpretation of the experimental findings. The lithiation of both Si and Ge have been proven to be highly influenced by factors such as particle morphology and cycling conditions. Particular attention must be given to the process of inhomogeneous lithiation that leaves place to the stabilization of metastable and/or non-thermodynamic phases. Also, there is a risk of degradation during the sample processing prior characterization, thus, implementing *operando* measurements is vital. Finally, a better understanding of novel phases such as siloxene and germanane, will support their implementation as battery materials and will provide alternative routes for overcoming the challenges related with the lithiation of Si and Ge-based materials. If the hypothesis of the Li intercalation is proved right, the conventional paradigms for the processes taking place will be changed, opening the possibility for the study of a whole new family of materials (Xens) from a totally new perspective.

Acknowledgments

The authors thank the financial support of the French National Research Agency (STORE-EX Labex Project ANR-10-LABX-76-01). The authors thank Nicolas LOUVAIN and Léa Daenens (ICG) for their help with Raman operando measurements.

ORCID

L. C. Loaiza https://orcid.org/0000-0002-3164-4509
N. Dupré https://orcid.org/0000-0002-0687-9357
L. Madec https://orcid.org/0000-0002-7681-1681
L. Monconduit https://orcid.org/0000-0003-3698-856X
V. Seznec https://orcid.org/0000-0001-5233-5943

References

1. L. C. Loaiza, L. Monconduit, and V. Seznec, *Small*, 19052601 (2020).
2. L. Zhao, D. J. Dvorak, and M. N. Obrovac, *J. Power Sources*, **332**, 290 (2016).
3. L. C. Loaiza, L. Monconduit, and V. Seznec, *Batter. Supercaps*, **3**, 1 (2020).
4. L. C. Loaiza, L. Monconduit, and V. Seznec, *J. Power Sources*, **417**, 99 (2019).
5. R. Fu, K. Zhang, R. Proietti, H. Huang, and Y. Xia, *Nano Energy*, **39**, 546 (2017).
6. R. Fu, Y. Li, Y. Wu, C. Shen, C. Fan, and Z. Liu, *J. Power Sources*, **432**, 65 (2019).
7. A. C. Serino, J. S. Ko, M. T. Yeung, J. J. Schwartz, C. B. Kang, S. H. Tolbert, R. B. Kaner, B. S. Dunn, and P. S. Weiss, *ACS Nano*, **11**, 7995 (2017).
8. X. Zhang, X. Qiu, D. Kong, L. Zhou, Z. Li, X. Li, and L. Zhi, *ACS Nano*, **11**, 7476 (2017).
9. K. Xu, L. Ben, H. Li, and X. Huang, *Nano Res.*, **8**, 2654 (2015).
10. W. Zhang, L. Sun, J. M. V. Nsanzimana, and X. Wang, *Adv. Mater.*, **30**, 1705523 (2018).
11. L. C. Loaiza, N. Louvain, B. Fraisse, A. Boulaoued, A. Iadecola, P. Johansson, L. Stievano, V. Seznec, and L. Monconduit, *J. Phys. Chem. C*, **122**, 3709 (2018).
12. M. Morcrette, Y. Chabre, G. Vaughan, G. Amatucci, J. B. Leriche, S. Patoux, C. Masquelier, and J. M. Tarascon, *Electrochim. Acta*, **47**, 3137 (2002).
13. L. Dupont, L. Laffont, S. Grugeon, S. Laruelle, V. Bodenez, and J. M. Tarascon, *ECS Trans.*, **3**, 139 (2007).
14. T. K.-J. Köster, E. Salager, A. J. Morris, B. Key, V. Seznec, M. Morcrette, C. J. Pickard, and C. P. Grey, *Angew. Chemie - Int. Ed.*, **50**, 12591 (2011).
15. R. Gao, J. Tang, K. Terabe, X. Yu, T. Sasaki, A. Hashimoto, K. Asano, M. A. Suzuki, and K. Nakura, *Chem. Phys. Lett.*, **730**, 198 (2019).
16. P. Lanz and P. Novak, *J. Electrochem. Soc.*, **161**, A1555 (2014).
17. L. A. Stearns, J. Gryko, J. Diefenbacher, G. K. Ramachandran, and P. F. McMillan, *J. Solid State Chem.*, **173**, 251 (2003).
18. A. J. Morris, C. P. Grey, and C. J. Pickard, *Phys. Rev. B*, **90**, 054111 (2014).
19. G. A. Tritsaris, E. Kaxiras, S. Meng, and E. Wang, *Nano Lett.*, **13**, 2258 (2013).
20. G. Vogg, M. S. Brandt, L. J.-P. Meyer, M. Stutzmann, Z. Hajnal, B. Szücs, and T. Rauenheim, *MRS Proc.*, **667**, 2 (2001).
21. P. Pazhamalai, K. Krishnamoorthy, S. Sahoo, V. K. Mariappan, and S.-J. Kim, *ACS Appl. Mater. Interfaces*, **11**, 624 (2018).
22. J. Graetz, C. C. Ahn, R. Yazami, and B. Fultz, *Electrochem. Solid State Lett.*, **6**, A194 (2003).
23. C. Forestier, P. Jankowski, A. Wizner, C. Davoisne, G. Gachot, L. Sannier, S. Grugeon, P. Johansson, M. Armand, and S. Laruelle, *J. Power Sources*, **345**, 212 (2017).
24. N. Dupré, P. Moreau, E. De Vito, L. Quazuguel, M. Boniface, A. Bordes, C. Rudisch, P. Bayle-Guillemaud, and D. Guyomard, *Chem. Mater.*, **28**, 2557 (2016).
25. S. Yamanaka, H. Matsu-ura, and M. Ishikawa, *Mater. Res. Bull.*, **31**, 307 (1996).
26. C.-M. Park, W. Choi, Y. Hwa, J. H. Kim, G. Jeong, and H.-J. Sohn, *J. Mater. Chem.*, **20**, 4854 (2010).
27. H. Nakano, *J. Ceram. Soc. Japan*, **122**, 748 (2014).
28. J. Yu, J. Gao, F. Xue, X. Yu, H. Yu, X. Dong, H. Huang, A. Ding, X. Quan, and G. Cao, *RSC Adv.*, **5**, 68714 (2015).
29. Y. Li et al., *Adv. Sci.*, 15000571 (2015).
30. T. Kennedy, M. Brandon, F. Laffir, and K. M. Ryan, *J. Power Sources*, **359**, 601 (2017).
31. Z. Xu and J. F. Stebbins, *Solid State Nucl. Magn. Reson.*, **5**, 103 (1995).
32. A. S. Cattaneo, S. Dupke, A. Schmitz, J. P. Badillo, M. Winter, H. Wiggers, and H. Eckert, *Solid State Ionics*, **249–250**, 41 (2013).
33. S. Dupke, T. Langer, R. Potgen, M. Winter, S. Passerini, and H. Eckert, *Phys. Chem. Chem. Phys.*, **14**, 6496 (2012).
34. K. Ogata, E. Salager, C. J. Kerr, A. E. Fraser, C. Ducati, A. J. Morris, S. Hofmann, and C. P. Grey, *Nat. Commun.*, **5**, 3217 (2014).
35. B. Key, M. Morcrette, J.-M. Tarascon, and C. P. Grey, *J. Am. Chem. Soc.*, **133** (2011).
36. B. Key, R. Bhattacharyya, M. Morcrette, V. Seznec, J. M. Tarascon, and C. P. Grey, *J. Am. Chem. Soc.*, **131**, 9239 (2009).
37. B. Mortazavi, A. Dianat, G. Cuniberti, and T. Rabczuk, *Electrochim. Acta*, **213**, 865 (2016).
38. H. Jung et al., *Chem. Mater.*, **27**, 1031 (2015).
39. W. Tang, Y. Liu, C. Peng, M. Y. Hu, X. Deng, M. Lin, J. Z. Hu, and K. P. Loh, *J. Am. Chem. Soc.*, **137**, 2600 (2015).

40. L. Baggetto, E. J. M. Hensen, and P. H. L. Notten, *Electrochim. Acta*, **55**, 7074 (2010).
41. L. Baggetto and P. H. L. Notten, *J. Electrochem. Soc.*, **156**, A169 (2009).
42. S. Yoon, C.-M. Park, and H.-J. Sohn, *Electrochem. Solid-State Lett.*, **11**, A42 (2008).
43. L. Y. Lim, S. Fan, H. H. Hng, and M. F. Toney, *Adv. Energy Mater.*, **5**, 1500599 (2015).
44. L. Y. Lim, S. Fan, H. H. Hng, and M. F. Toney, *J. Phys. Chem. C*, **119**, 22772 (2015).
45. L. Y. Lim, N. Liu, Y. Cui, and M. F. Toney, *Chem. Mater.*, **26**, 3739 (2014).
46. N. Dupré, M. Cuisinier, and D. Guyomard, *Electrochem. Soc. Interface*, **20**, 61 (2011).
47. L. M. Scherf, A. J. Karttunen, O. Pecher, P. C. M. M. Magusin, C. P. Grey, and T. F. Fässler, *Angew. Chemie Int. Ed.*, **55**, 1075 (2016).
48. D. K. Sharma, S. Kumar, A. Laref, and S. Auluck, *Comput. Condens. Matter*, **16**, e00314 (2018).
49. R. Bhuvaneswari, V. Nagarajan, and R. Chandiramouli, *Mater. Res. Express*, **6**, 035504 (2019).
50. J. D. Corbett, *Angew. Chemie - Int. Ed.*, **39**, 670 (2000).
51. J. Evers and G. Oehlinger, *Angew. Chemie - Int. Ed.*, **40**, 1050 (2001).
52. X. Lin and J. Ni, *Phys. Rev. B - Condens. Matter Mater. Phys.*, **86**, 075440 (2012).
53. J. Zhuang, X. Xu, G. Peleckis, W. Hao, S. X. Dou, and Y. Du, *Adv. Mater.*, 16067161 (2017).
54. H. Oughaddou, H. Enriquez, M. R. Tchalala, H. Yildirim, A. J. Mayne, A. Bendounan, G. Dujardin, M. A. Ali, and A. Kara, *Prog. Surf. Sci.*, **90**, 46 (2015).
55. V. V. Kulish, O. I. Malyi, M.-F. Ng, Z. Chen, S. Manzhos, and P. Wu, *Phys. Chem. Chem. Phys.*, **16**, 4260 (2014).